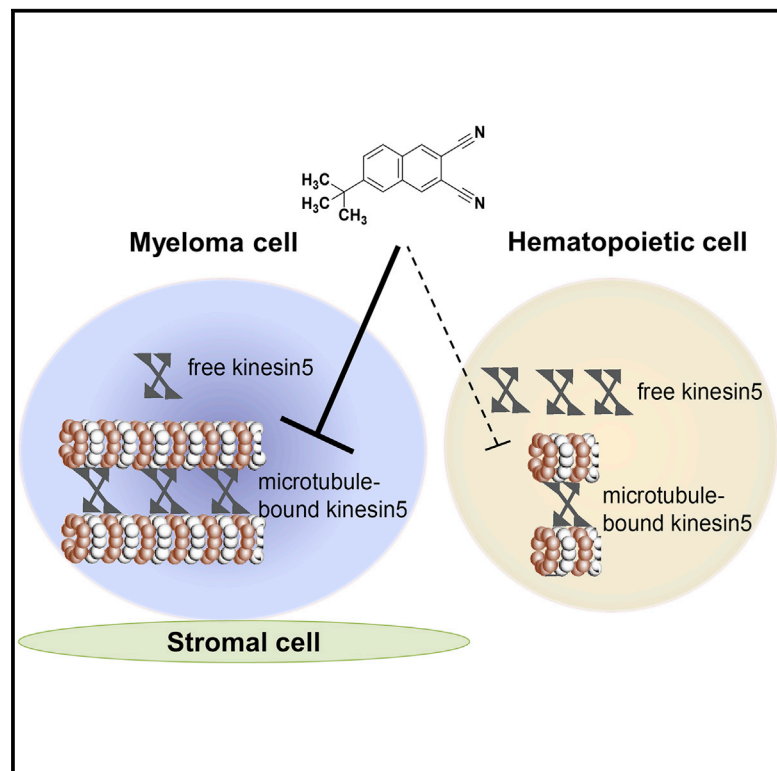


Niche-Based Screening in Multiple Myeloma Identifies a Kinesin-5 Inhibitor with Improved Selectivity over Hematopoietic Progenitors

Graphical Abstract



Authors

Shrikanta Chattopadhyay,
Alison L. Stewart, ..., David T. Scadden,
Stuart L. Schreiber

Correspondence

schattopadhyay@partners.org (S.C.),
stuart_schreiber@harvard.edu (S.L.S.)

In Brief

Discovering therapeutics for multiple myeloma (MM) is challenging due to its complex genome and stroma-induced drug resistance. Chattopadhyay et al. use MM-stroma co-cultures to identify compounds that overcome stromal resistance. One compound specifically targets microtubule-bound, phosphorylated Eg5, which is higher in MM than hematopoietic cells, revealing a therapeutic strategy.

Highlights

- Phenotypic screening identifies compounds that overcome stromal resistance in MM
- Compound BRD9876 only inhibits microtubule-bound Eg5, which is high in MM cells
- This unusual mode of action enables MM over hematopoietic progenitor selectivity
- Thus, compounds identified here can discover “druggable” vulnerabilities within MM

Accession Numbers

GSE64178



Niche-Based Screening in Multiple Myeloma Identifies a Kinesin-5 Inhibitor with Improved Selectivity over Hematopoietic Progenitors

Shrikanta Chattopadhyay,^{1,2,3,*} Alison L. Stewart,¹ Siddhartha Mukherjee,⁴ Cherrie Huang,^{1,2} Kimberly A. Hartwell,⁵ Peter G. Miller,^{6,15} Radhika Subramanian,⁷ Leigh C. Carmody,¹ Rushdia Z. Yusuf,^{2,3} David B. Sykes,^{2,3} Joshiawa Paulk,^{1,9} Amedeo Vetere,¹ Sonia Vallet,³ Loredana Santo,³ Diana D. Cirstea,⁸ Teru Hideshima,⁸ Vlado Dančik,¹ Max M. Majireck,^{1,9} Mahmud M. Hussain,^{1,9,16} Shambhavi Singh,^{1,9} Ryan Quiroz,^{1,10} Jonathan Iaconelli,^{1,11} Rakesh Karmacharya,^{1,11,12} Nicola J. Tolliday,¹ Paul A. Clemons,¹ Malcolm A.S. Moore,¹³ Andrew M. Stern,^{1,14} Alykhan F. Shamji,¹ Benjamin L. Ebert,^{8,15} Todd R. Golub,^{5,8,16} Noopur S. Raje,³ David T. Scadden,^{2,3,6,9} and Stuart L. Schreiber^{1,9,16,*}

¹Center for the Science of Therapeutics / Center for the Development of Therapeutics, Broad Institute, Cambridge, MA 02142, USA

²Center for Regenerative Medicine, Massachusetts General Hospital, Boston, MA 02114, USA

³Cancer Center, Massachusetts General Hospital, Boston, MA 02114, USA

⁴Department of Medicine and Irving Cancer Research Center, Columbia University School of Medicine, New York, NY 10032, USA

⁵Cancer Program, Broad Institute, Cambridge, MA 02142, USA

⁶Harvard Medical School, Boston, MA 02115, USA

⁷Chemistry and Cell Biology, Rockefeller University, New York, NY 10065, USA

⁸Dana-Farber Cancer Institute, Boston, MA 02115, USA

⁹Harvard University, Cambridge, MA 02138, USA

¹⁰University of California, Los Angeles, Los Angeles, CA 90095, USA

¹¹Center for Human Genetic Research, Massachusetts General Hospital, Boston, MA 02114, USA

¹²Schizophrenia and Bipolar Disorder Program, McLean Hospital, Belmont, MA 02478, USA

¹³Cell Biology, Memorial Sloan Kettering Cancer Center, New York, NY 10065, USA

¹⁴Drug Discovery Institute, University of Pittsburgh, Pittsburgh, PA 15260, USA

¹⁵Division of Hematology, Brigham and Women's Hospital, Boston, MA 02115, USA

¹⁶Howard Hughes Medical Institute, Broad Institute, Cambridge, MA 02142, USA

*Correspondence: schattopadhyay@partners.org (S.C.), stuart_schreiber@harvard.edu (S.L.S.)

<http://dx.doi.org/10.1016/j.celrep.2015.01.017>

This is an open access article under the CC BY-NC-ND license (<http://creativecommons.org/licenses/by-nc-nd/3.0/>).

SUMMARY

Novel therapeutic approaches are urgently required for multiple myeloma (MM). We used a phenotypic screening approach using co-cultures of MM cells with bone marrow stromal cells to identify compounds that overcome stromal resistance. One such compound, BRD9876, displayed selectivity over normal hematopoietic progenitors and was discovered to be an unusual ATP non-competitive kinesin-5 (Eg5) inhibitor. A novel mutation caused resistance, suggesting a binding site distinct from known Eg5 inhibitors, and BRD9876 inhibited only microtubule-bound Eg5. Eg5 phosphorylation, which increases microtubule binding, uniquely enhanced BRD9876 activity. MM cells have greater phosphorylated Eg5 than hematopoietic cells, consistent with increased vulnerability specifically to BRD9876's mode of action. Thus, differences in Eg5-microtubule binding between malignant and normal blood cells may be exploited to treat multiple myeloma. Additional steps are required for further therapeutic development, but our results indicate that unbiased chemical biology approaches can identify therapeutic

strategies unanticipated by prior knowledge of protein targets.

INTRODUCTION

Multiple myeloma (MM) is an incurable malignancy that caused more than 80,000 deaths in 2012 worldwide (Ferlay et al., 2013). Novel therapeutic approaches are desperately needed, but target-based drug development against this disease is challenging due to complex genomic alterations including multiple driver mutations even within the same individual (Lohr et al., 2014). An alternative phenotypic approach to therapeutic discovery is to define a cellular phenotype representative of the disease and to use small-molecule screening to discover simultaneously relevant therapeutic targets and lead compounds. The success of this general approach is shown by the observation that the majority of first-in-class drugs approved by the US Food and Drug Administration (FDA) between 1999 and 2008 came from phenotypic approaches despite the dominance of target-based drug discovery during that period (Swinney and Anthony, 2011). In MM, novel therapeutic discovery has occurred largely using the phenotypic approach. Lactacystin, a natural product with phenotypic effects in cancer cells, was used to discover that the proteasome could be targeted selectively by engaging a catalytic β -subunit N-terminal threonine

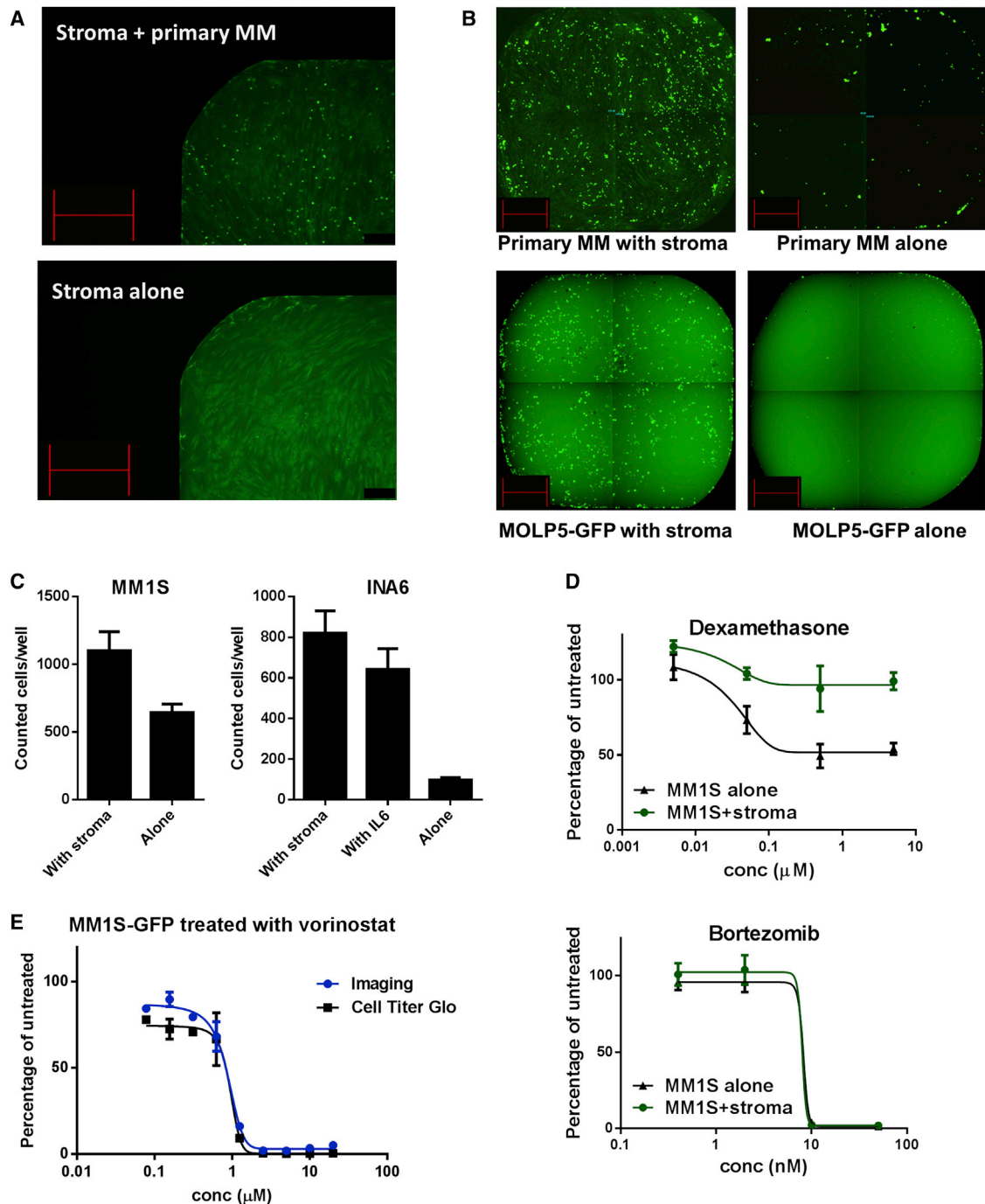


Figure 1. Assays to Identify Small-Molecule Inhibitors of Multiple Myeloma within Its Stromal Niche

(A) Different Calcein AM staining characteristics of multiple myeloma (MM) cells and stromal cells. Primary bone marrow stroma cells (stroma) were either grown alone (bottom) or co-cultured with primary CD138+ MM (top) and stained with the vital dye Calcein AM. Differences in cell shape, size, and fluorescence intensity were used to distinguish the two cell types. The scale bar represents 500 μm .

(B) Stroma dependence of primary MM and MOLP5 cells. Top: primary CD138+ MM cells were cultured with stroma (left) or alone in media (right) in 384-well plates and then stained with Calcein AM and imaged. Bottom: GFP-labeled MOLP5 cells were similar grown with stroma (left) or alone (right) for 5 days and then imaged. The scale bar represents 500 μm .

(C) Enhanced growth of MM1S and INA6 cells with stroma. Left: GFP-labeled MM1S cells were cultured with stromal cells or alone for 5 days and then GFP+ cells were counted using the MetaXpress software (Molecular Devices). Right: GFP-labeled INA6 cells were cultured with stroma, in media with IL6, or in media alone for 5 days and then quantified by imaging. Data are averages (avg) \pm SEM (n = 14).

(legend continued on next page)

(Fenteany et al., 1995). This knowledge accelerated the discovery and development of bortezomib from previously unselective peptide aldehydes (Adams et al., 1998), and subsequently, bortezomib transformed the treatment of MM (Richardson et al., 2005). The development of thalidomide and its analogs against MM also followed phenotypic observations of thalidomide's effects on angiogenesis and immune function (Bartlett et al., 2004). Based on these encouraging precedents, we undertook a phenotypic screening approach to systematically discover compounds that uncover new therapeutic strategies against MM.

In 95% of MM cases, the malignant cells are restricted to the bone marrow, where interactions with the stromal niche are thought to be critical for their survival (Hideshima et al., 2007) and for drug resistance to traditional chemotherapy drugs (Meads et al., 2008). The ability to overcome resistance factors from bone marrow stromal cells (BMSCs) is now considered an obligate requirement for any novel therapeutic agent against MM (Dalton and Anderson, 2006). Agents like bortezomib, thalidomide, and lenalidomide overcome BMSC resistance in vitro (Hideshima et al., 2000, 2001) and achieve complete, durable responses in vivo, resulting in greatly improved survival (Hideshima et al., 2007). McMillin and colleagues used an assay in which labeled MM cell lines are co-cultured with BMSCs and determined that the anti-MM activities of a variety of FDA-approved and bioactive compounds are attenuated by BMSCs (McMillin et al., 2010). We adapted this BMSC-MM co-culture assay in 384-well plates for high-throughput screening to identify compounds that overcome the stroma-induced drug-resistance phenotype in MM. Because hematological toxicity is common for anti-MM agents, we prioritized compounds with selectivity over human hematopoietic progenitors to identify those with improved toxicity profiles. One such compound, BRD9876, was discovered to be a distinctive kinesin-5 (Eg5; kinesin spindle protein; KIF11) inhibitor that specifically targets microtubule-bound Eg5, allowing greater selectivity over hematopoietic cells. An Eg5 inhibitor, ARRY-520, is showing promising, durable responses in MM (Shah et al., 2011), but its use is limited by hematological toxicity. We report here a novel mechanism of Eg5 inhibition that could preserve anti-MM efficacy while mitigating potentially life-threatening hematological toxicity during MM treatment.

RESULTS

Screening for Compounds that Overcome Stromal Resistance in Multiple Myeloma

To recapitulate the MM niche in vitro, we used primary human BMSCs isolated from hip replacement samples, removed for non-cancerous indications. We co-cultured primary MM cells with these BMSCs and stained them with the vital dye Calcein AM, utilizing intensity and shape differences to distinguish and

quantify the two cell types in the MetaXpress software (Molecular Devices). Primary MM cells displayed round, bright staining (Figure 1A), whereas BMSCs alone appeared as dull, spindle-shaped objects. Co-culture with BMSCs maintained the viability of CD138(+) primary MM cells >5-fold better than culture media alone (Figure 1B), confirming previously observed stroma dependence of primary MM (Zlei et al., 2007). To recapitulate this behavior in a cell line amenable to high-throughput screening, the stroma-dependent MM cell line MOLP5 (Matsuo et al., 2000), stably expressing GFP, was similarly grown alone or in co-culture with stroma in 384-well plates. A similar ~7-fold increase in GFP(+) MOLP5 cells was observed with stromal co-culture (Figure 1B) using image-based quantification, making this an attractive physiologically relevant high-throughput assay to screen for small-molecule inhibitors of MM within its niche.

To determine the impact of stroma on the activity of small molecules, we chose two other MM cell lines (MM.1S cells and IL6-dependent INA6 cells) that grow with or without BMSCs. MM.1S (MM1S) cells grow well alone but double their proliferation in the presence of stromal cells (Hideshima et al., 2001; Figure 1C). The survival of INA6 cells is dependent on the presence of high concentrations of IL6 or on co-culture with BMSCs (Chatterjee et al., 2002). The effect of BMSC co-culture on small-molecule activity was confirmed in these cells. Dexamethasone inhibited the growth of MM1S grown alone, but not in the presence of stroma (Figure 1D). In contrast, bortezomib, which overcomes microenvironment resistance (Hideshima et al., 2001), is equally active in the presence or absence of stroma, consistent with its ability to induce durable complete responses in vivo. Thus, small molecules that overcome stromal resistance can be identified using MM1S and INA6 cells with or without stromal co-culture.

Assay optimization was achieved using vorinostat as a positive control. The image-based viability assay and the Cell-Titer-Glo assay (Promega; measures cellular ATP content) produced similar dose-response curves (Figure 1E) with vorinostat. The Z' factor, a statistical test of assay robustness that incorporates SDs and differences of means of negative and positive controls (Zhang et al., 1999), was consistently above 0.5 for the MOLP5-BMSC imaging assay, confirming its suitability for high-throughput screening.

We chose the MOLP5-BMSC co-culture assay as the primary assay for screening small molecules to identify compounds that either overcome stromal resistance or are active against stroma-dependent MM. A library of 25,280 compounds comprising FDA-approved drugs, bioactive compounds, natural products, commercial vendor compounds, kinase-biased compounds, chromatin-biased compounds, and compounds synthesized at the Broad Institute using diversity-oriented synthesis (DOS) (Nielsen and Schreiber, 2008) were tested in duplicate in the primary assay and showed good reproducibility (Figure 2A). Compounds that inhibited MOLP5 growth with Z scores ≤ -2 relative to DMSO controls in both replicates were considered "hits".

(D) Stroma confers drug resistance to dexamethasone. MM1S-GFP cells were exposed to varying concentrations of dexamethasone (top) or bortezomib (bottom) for 3 days in the presence (green) or absence (black) of stroma and quantified by imaging. Data are avg \pm SEM (n = 8).

(E) Viability measurements by imaging are equivalent to the Cell-Titer-Glo reagent. MM1S-GFP cells growing alone were exposed to varying concentrations of vorinostat for 3 days, following which remaining viable cells were quantified by imaging (blue) or using the Cell-Titer-Glo reagent (black) that measures ATP content. Data are avg \pm SEM (n = 2).

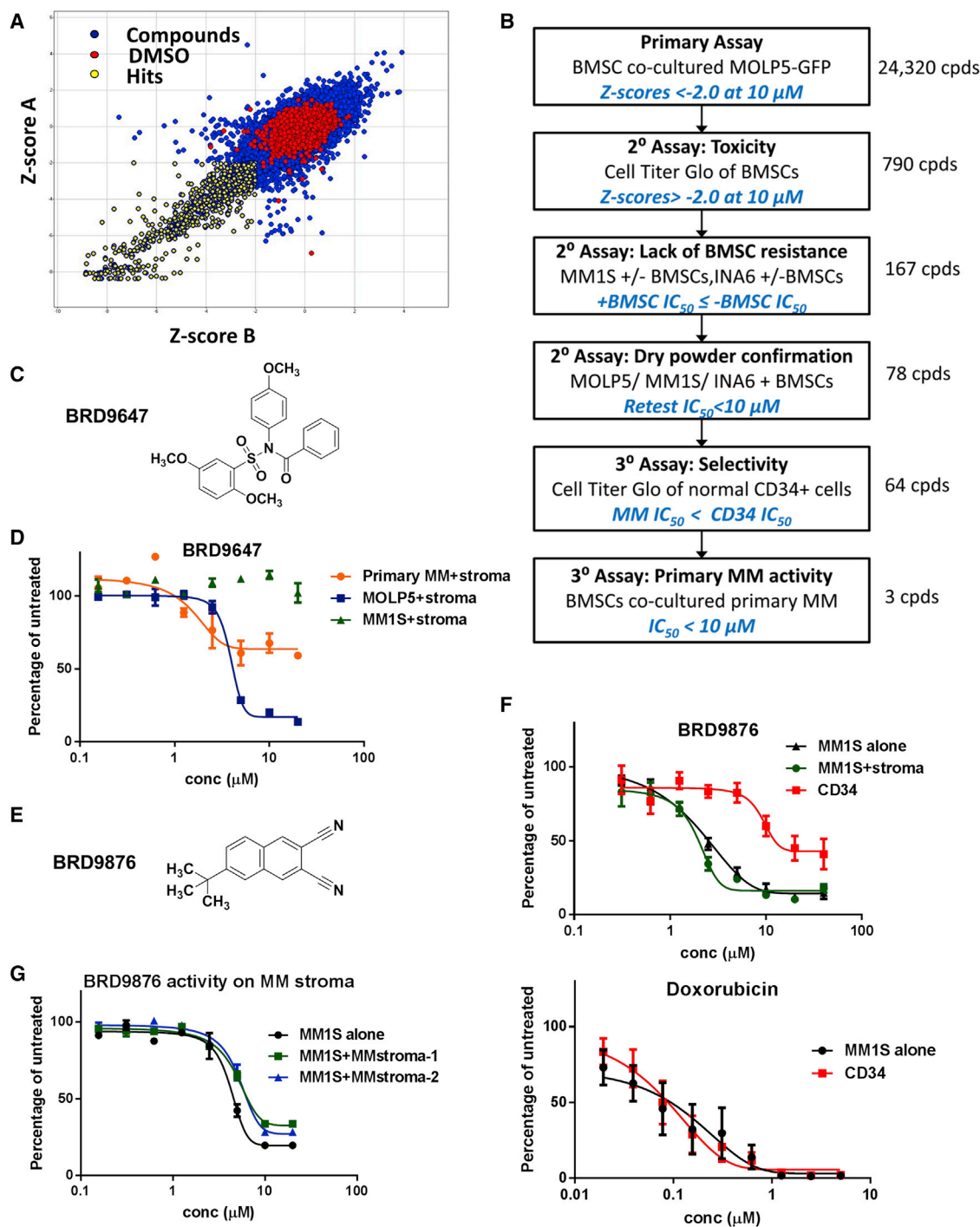


Figure 2. High-Throughput Screen Identifies Small Molecules that Overcome Stromal Resistance

(A) Summary of screening data for both replicates of 24,320 compounds (blue) on MOLP5-GFP co-cultured with stroma, depicted as Z scores of DMSO controls (red). Compounds with Z score < -2.0 in both replicates were considered “hits” (yellow).

(B) Schematic summarizing the experimental approaches used to filter high-priority compounds that overcome bone marrow stromal cell (BMSC) resistance. Criteria used for each step are in blue, and numbers of compounds tested in each step are on the right.

(C) Structure of a hit compound BRD9647.

(D) BRD9647 is selective for stroma-dependent MM cells. MM1S-GFP (green) or stroma-dependent MOLP5-GFP (blue) and primary MM cells (orange) were grown with stroma and exposed to eight doses of BRD9647 for 3 days and then viable cells were quantified by imaging. Data are avg \pm SEM (n = 2).

(legend continued on next page)

We developed a prioritization schema to identify compounds of high interest (Figure 2B). We tested hits on BMSCs growing alone to exclude compounds with non-specific toxicity. Then, to exclude compounds that are susceptible to stromal resistance (like dexamethasone), we tested hits at eight doses on MM1S and INA6 cells with or without BMSCs. Compounds with IC_{50} with BMSCs $\leq IC_{50}$ without BMSCs were validated by ordering them in powder form and then retesting in primary and secondary assays. We identified 60 compounds that reproducibly inhibited MM growth, did not demonstrate non-specific toxicity, and could overcome stromal resistance (Table S1). Because hematological toxicity is common for most MM inhibitors, we then tested compounds on human CD34+ hematopoietic progenitors growing in serum-free liquid culture media, an assay predictive for in vivo hematological toxicity (Olaharski et al., 2009). Only a few compounds demonstrated greater inhibition of MM growth than hematopoietic growth (Table S1), and of these, three compounds were tested on primary MM cells co-cultured with BMSCs.

We identified compounds with unique selectivity patterns. A sulfonamide BRD9647 (Figure 2C) displayed selective inhibition of stroma-dependent MOLP5 and primary MM cells, but not stroma-independent cell lines like MM1S (Figure 2D). This compound suppressed the viability of three out of six primary MM samples (Figures S1A and S1B) at greater than or equal to two concentrations $\leq 10 \mu\text{M}$ ($p < 0.05$ by t test), but the maximal effect did not exceed 50% in any sample, suggesting primarily cytostatic effects. A chromanone BRD2588 (Figure S1C) displayed *enhanced* activity in the presence of stroma (the opposite of dexamethasone). In contrast to vorinostat (Figure S1D), a hydrazone-containing hydroxamic acid BRD2318 displayed selectivity for IL6-dependent INA6 (Figure S1E).

We focused our attention on a naphthalene bis-nitrile BRD9876 (Figure 2E) that inhibited MM1S growth equally with or without BMSCs (like bortezomib) with a modest (~ 4 -fold) but significant selectivity over normal CD34+-derived hematopoietic cells (MM1S IC_{50} : $2.2 \pm 0.5 \mu\text{M}$; CD34 IC_{50} : $9.2 \pm 2 \mu\text{M}$; Figure 2F). In contrast, no MM over CD34 selectivity was observed for most tested compounds such as doxorubicin (Figure 2F), which causes significant hematological toxicity in vivo in MM patients (Alberts and Salmon, 1975). BRD9876 was able to overcome, in MM1S cells, stromal resistance of BMSCs from MM bone marrow aspirates (Figure 2G), but only minimal effects were observed with BRD9876 against primary MM cells (Figure S2A). This was initially concerning, but we observed that primary MM cells do not proliferate in vitro, even in the presence of stroma in contrast to cell lines like MM1S (Figure S2B). Consistent with the lack of proliferation, primary MM cells were insensitive to the anti-mitotic Eg5 inhibitor ARRY-520 (Figure S2C), which is efficacious against MM in vivo, although they were sensitive to bortezomib that induces apoptosis (Figure S2D). These data suggested that BRD9876 may be specific for cycling MM cells. Because BRD9876 was able to inhibit diverse MM cell

lines, overcome stromal resistance, and display selectivity over hematopoietic progenitors, we undertook studies to identify its mechanism of action.

Mitotic Kinesin-5 Is the Target of BRD9876

We first synthesized or purchased structural analogs of BRD9876 with the goal of immobilizing the compound on beads for affinity purification of protein-binding partners. However, all structural analogs of BRD9876 (Figure S3) were either less active against MM1S cells or lost selectivity between MM1S and CD34 blood cells. We therefore switched our attention to understanding the functional effects of BRD9876 on MM1S cells. Gene-expression analysis of MM1S cells treated for 6 hr with BRD9876 revealed sparse changes—only ten genes changed in expression >2 -fold. Network analysis of genes with >1.5 -fold changes revealed no significant relationship between genes (Figure S4A). We turned to analyzing individual genes, focusing on the top downregulated gene, ID1 (Figure 3A). We queried the Connectivity Map database (Lamb et al., 2006), which contains over 7,000 gene-expression profiles of bioactive compounds, for compounds that downregulate ID1 expression. The top ten compounds that downregulate ID1 included the anti-mitotic paclitaxel (Figure S4B). This finding, in addition to literature reports of ID1 expression being associated with abnormal mitoses (Man et al., 2008), suggested possible anti-mitotic effects of BRD9876. Cell-cycle analysis of MM1S treated with $10 \mu\text{M}$ BRD9876 revealed rapid arrest of cells at the G2/M phase, starting as early as 2 hr of treatment (Figure 3B). In contrast, CD34 hematopoietic cells treated with BRD9876 showed markedly less G2/M arrest (Figure 3C), albeit these cultures contained fewer cycling cells.

To determine whether treated MM1S cells arrested at G2 or entered mitosis, we stained the mitotic spindle protein α -tubulin. Not only were a significant number of cells arrested in mitosis, but they uniformly exhibited an aberrant mono-astral mitotic spindle (Figure 3D). Mono-astral spindles are a characteristic feature of inhibitors of mitotic kinesin-5 (Eg5), first demonstrated with the Eg5 inhibitor monastrol (Mayer et al., 1999) but later observed with polo-like kinase or aurora kinase inhibitors (Tillemont et al., 2009). Therefore, we tested Eg5 activity in a microtubule-gliding assay in which recombinant full-length Eg5 drives motility of rhodamine-labeled microtubules (Mayer et al., 1999). In the presence of $1 \mu\text{M}$ BRD9876, Eg5-mediated microtubule gliding was completely arrested (Figure 3E). Inhibition of Eg5 activity was further confirmed in a microtubule-stimulated ATPase assay of the recombinant Eg5 motor domain that demonstrated that BRD9876 was an ATP non-competitive inhibitor of Eg5 (Figures 3F and S5A).

Novel BRD9876 Resistance Mutation Suggests a Distinct Allosteric Binding Site

Eg5 inhibitors such as ARRY-520 have demonstrated promising durable responses in MM (Shah et al., 2011), prompting a

(E) Structure of another hit compound BRD9876.

(F) BRD9876 overcomes stroma resistance and spares hematopoietic progenitors. MM1S-GFP cells were either grown alone (black) or co-cultured with stroma (green) and, along with cells derived from CD34+ hematopoietic progenitors (red), exposed to eight doses of BRD9876 (top) or doxorubicin (bottom) for 3 days. Viable cells were quantified by imaging (MM1S) or with Cell Titer Glo (CD34). Data are $\text{avg} \pm \text{SEM}$ ($n \geq 6$).

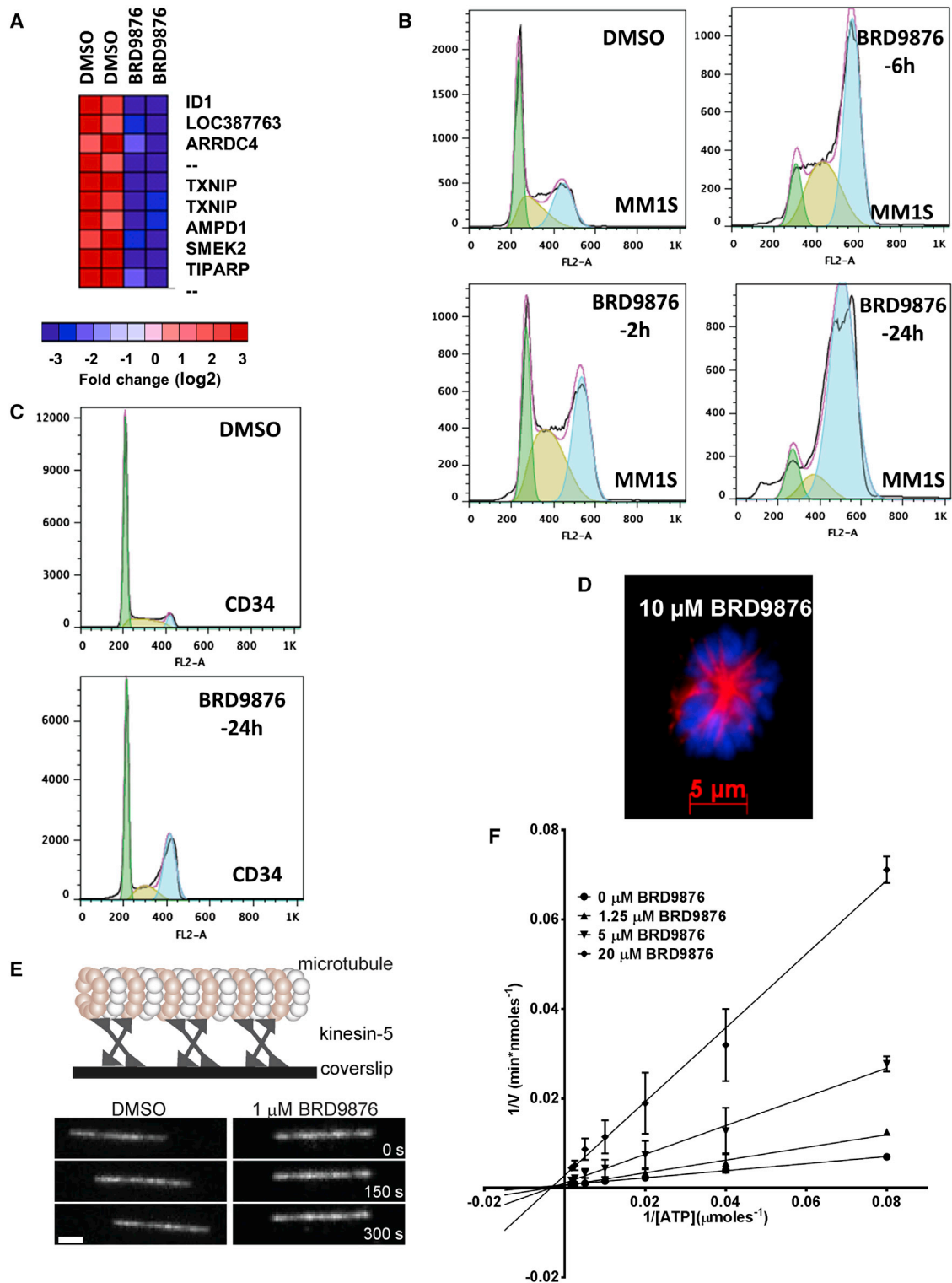


Figure 3. Novel Small Molecule BRD9876 Is a Mitotic Kinesin-5 Inhibitor

(A) Affymetrix gene-expression analysis of MM1S cells treated with 10 μM BRD9876 for 6 hr compared with DMSO-treated cells identifies ID1 as the top downregulated gene. The top ten Affymetrix probe sets downregulated by BRD9876 treatment are depicted here.

(B) Cell-cycle analysis of MM1S cells treated with DMSO (top left panel) or 10 μM BRD9876 (remaining panels) for indicated time points. Staining intensity of the DNA stain propidium iodide (corresponding to ploidy) is depicted on the x axis and numbers of cells on the y axis.

(legend continued on next page)

phase-III registration trial (Owens, 2013). Current clinical Eg5 inhibitors such as ispinesib and ARRY-520 bind the monastrol-binding loop L5 region on Eg5 (Talapatra et al., 2012; Woessner et al., 2009) and exhibit severe hematological toxicity (Burriss et al., 2011; Shah et al., 2011) requiring myeloid growth factor support. Because BRD9876 exhibited selectivity between MM and hematopoietic cells, we reasoned that BRD9876 may have a different mode of Eg5 inhibition. To explore this, MM1S cells were raised to be resistant to BRD9876 by serial exposure to increasing compound concentrations. Consistent with our reasoning, an MM1S subline, MM1S-BRD9876R, had no cross-resistance to ispinesib (Figure 4A). Sequencing Eg5 cDNA from MM1S-BRD9876R revealed a previously unreported heterozygous mutation (Figure 4B) that alters the amino acid residue at position 104 from tyrosine (Y) to cysteine (C), suggesting a dominant drug-resistance allele. Intriguingly, this mutation is distant from the known binding site of existing Eg5 inhibitors (Figure 4C), suggesting a distinct allosteric binding site for BRD9876. Resistance to existing Eg5 inhibitors like ispinesib and monastrol is mediated by a loop L5 mutation at position 130 aspartate (D130; Figure 4C; Luo et al., 2007). To confirm the unique resistance mechanism of BRD9876, we generated recombinant Eg5 motor domain constructs, containing the wild-type (WT) sequence, Y104C mutation, or D130V mutation. Enzymatic microtubule-stimulated ATPase activities were identical for all three constructs (Figure S5B). The Y104C mutant was completely resistant to BRD9876 (Figure 4D) while showing no alteration to ispinesib activity. In contrast, the D130V mutant conferred ~10-fold resistance to ispinesib and ~10-fold sensitization to BRD9876. To test whether the Eg5 mutations were sufficient to confer resistance in cells, we introduced lentiviral vectors containing C-terminal GFP-tagged Eg5 open reading frame (ORF) with the WT sequence or Y104C or D130V mutations into adherent SW48 cells, chosen because of a high efficiency of lentiviral transduction. Cells expressing the Y104C mutant construct were resistant to BRD9876, consistent with the dominant drug-resistant nature of this allele, whereas the D130V mutation conferred enhanced sensitivity (Figures 4E). In contrast, the D130V, but not the Y104C, construct imparted resistance to ispinesib. Similar results were obtained using doxycycline-inducible lentiviral constructs in MM1S cells (Figure S5C).

A recent report described a distinct Eg5 allosteric binding site between the $\alpha 4$ and $\alpha 6$ helices using a benzimidazole compound BI8 (Ulaganathan et al., 2013; Figure S5D). BI8 also bound, with weaker affinity, a site partially overlapping with the ispinesib L5 site. The crystal structure demonstrates that the Y104 residue participates in BI8 binding, forming a face-to-face stacking interaction with the trifluoromethylbenzyl group (Figure S5E). Indeed,

biochemical ATPase assays confirmed that the Y104C mutation conferred resistance to BI8 activity (Figure S5F). In contrast to BRD9876, neither the Y104C or D130V mutants imparted resistance to BI8 in cells expressing those constructs (Figure S5G), suggesting that BI8 occupies both allosteric sites at the higher concentrations required for cellular growth inhibition. These studies confirm that the Y104 residue is a bona fide member of the $\alpha 4/\alpha 6$ allosteric site and that BRD9876 binds exclusively to this site.

BRD9876 Specifically Inhibits Microtubule-Bound Kinesin-5

The Eg5 motor domain has basal ATPase activity in the absence of microtubules, but it is ~100-fold less efficient (Luo et al., 2004). Surprisingly, we found that BRD9876 was completely ineffective at inhibiting the basal ATPase activity of Eg5, in contrast to loop-L5-binding monastrol or $\alpha 4/\alpha 6$ -binding BI8 (Figure 5A), which showed greater activity against basal Eg5 ATPase activity.

To determine whether BRD9876 is selective for microtubule-bound Eg5 within cells, we altered the levels of microtubule-bound protein. Association of Eg5 with microtubules is regulated by CDK1-mediated phosphorylation of Eg5 threonine 927 (Blangy et al., 1995). CDK1 activity in turn is negatively regulated by the tyrosine kinase WEE1 and treatment with MK1775, a selective WEE1 inhibitor, forces CDK1 activation (Krajewska et al., 2013). MM1S cells treated with MK1775 showed increased levels of a faster migrating band (Figure 5B) in immunoblots with three different antibodies specific for threonine-927-phosphorylated Eg5 (phospho-Eg5) or the carboxy terminus (C-terminal Eg5) or amino terminus of Eg5 (N-terminal Eg5), confirming that the band contained full-length Eg5. The intensification of the lower band with increasing doses of MK1775 was markedly higher with the phospho-Eg5-specific antibody (Figure S6A), suggesting that this band primarily contains phospho-Eg5. The upper band showed a smaller increase in intensity caused by MK1775 treatment, suggesting that it contains only a minority of phospho-Eg5. The phospho-Eg5 antibody was confirmed to recognize phosphorylated Eg5 using phosphatase treatment, which reduced recognition of both bands by the phospho-Eg5 antibody, but not the C-terminal Eg5 antibody (Figure S6B). Electrophoretic mobility shifts can occur due to conformational changes, resulting in altered detergent binding in various proteins including Eg5 (Kim et al., 2010; Rath et al., 2009). The faster migrating electrophoresis pattern observed in Figure 5B may thus reflect conformational changes caused by forced CDK1-mediated Eg5 phosphorylation. Consistent with greater levels of phosphorylated, microtubule-bound Eg5, MK1775-pretreated

(C) Cell-cycle analysis of CD34+ cells cultured for 6 days and then treated with either DMSO (top) or 10 μ M BRD9876 (bottom) for 24 hr.

(D) Mono-astral mitotic pattern of MM1S cells treated with 10 μ M BRD9876 for 4 hr. The mitotic spindle protein α -tubulin is red, and DNA stained with Hoechst 33342 is blue.

(E) Effect of BRD9876 on the gliding of rhodamine-labeled microtubules on immobilized kinesin-5 (Eg5) tetramers. A schematic of the assay is depicted at the top. Images from a time-lapse sequence taken at indicated time points show that tetrameric Eg5 drives microtubule gliding with DMSO (left), but not with 1 μ M BRD9876 (right). The scale bar represents 2 μ m.

(F) BRD9876 is an ATP non-competitive Eg5 inhibitor. ATPase activity of recombinant Eg5 motor domain (residues 1–368) was measured with varying concentrations of ATP with/without increasing concentrations of BRD9876. The double reciprocal (Lineweaver-Burke) plots have a common intercept on the x axis, suggesting ATP non-competitive mode of inhibition. Data are avg \pm SEM of 6.

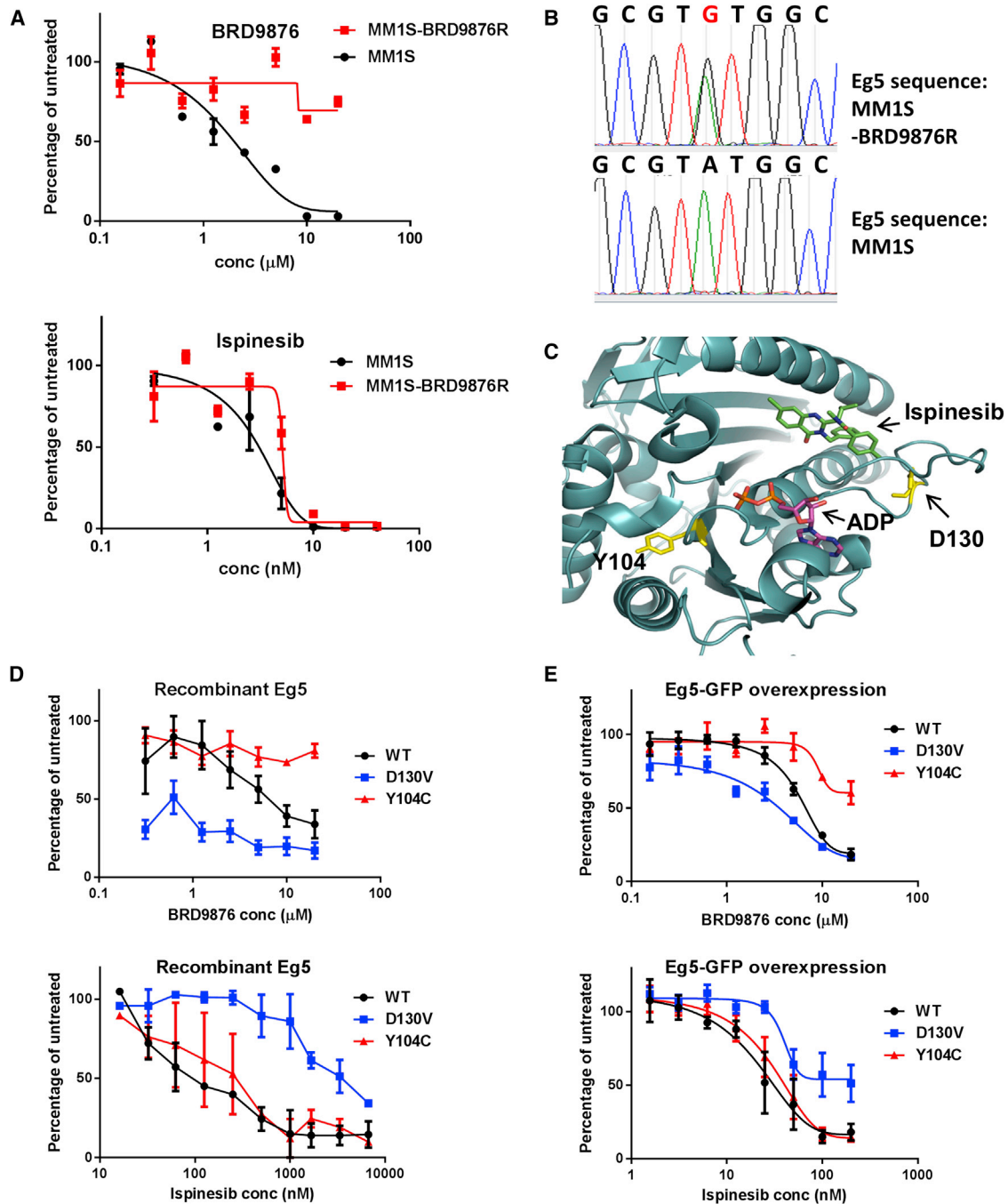


Figure 4. BRD9876 Has a Unique Mode of Resistance

(A) MM1S cells raised to be resistant to BRD9876 are not cross-resistant to an existing Eg5 inhibitor ispienesib. BRD9876-resistant MM1S cells (MM1S-BRD9876R; red) or parental MM1S cells (black) were exposed to varying doses of BRD9876 (top) or ispienesib (bottom) for 3 days. Data are avg \pm SEM (n = 3).

(B) BRD9876-resistant cells contain a novel heterozygous mutation. Eg5-coding region was PCR amplified from cDNA of MM1S-BRD9876R or MM1S cells and sequenced with traditional Sanger sequencing. A heterozygous missense mutation c.311A \rightarrow G, p.Tyr104Cys (Y104C) was found in resistant cells (top), but not in parental sensitive cells (bottom).

(C) X-ray crystal structure of the Eg5 motor domain bound to ispienesib (from PDB 4AP0), indicating that Y104 (yellow) is distant from the ispienesib-binding site. The D130 residue, mutations of which result in resistance to ispienesib, is also highlighted in yellow.

(D) Y104C mutation causes resistance to BRD9876, but not ispienesib, in Eg5 ATPase assays. Recombinant Eg5 motor domain (residues 1–368) proteins containing the wild-type sequence (black), the Y104C mutation (red), or the D130V mutation (blue) were incubated with microtubules and ATP for 10 min, in the

(legend continued on next page)

MM1S cells showed \sim 3-fold lower IC_{50} to BRD9876 (Figure 5C), whereas monastrol and BI8 activities were unchanged. The enhanced cytotoxic activity was paralleled by an \sim 3-fold lower BRD9876 EC_{50} for mitotic arrest in MK1775-co-treated MM1S cells (Figure 5D). The highly potent loop-L5-binding ispinesib also preferentially binds microtubule-free Eg5 (Lad et al., 2008) and, similar to monastrol, did not display changes in cytotoxicity (Figure S5C) or ability to induce mitotic arrest (Figure S5D) in MK1775-pretreated MM1S cells. Opposite effects on BRD9876 cytotoxic (Figure S5E) and mitotic (Figure S5F) activities were observed with the CDK1 inhibitor RO3306 (Vassilev et al., 2006). Similar shifts in BRD9876 cytotoxicity were observed in WSU-DLCL2 lymphoma cells induced to have higher (Figure S5G) or lower (Figure S5H) levels of phospho-Eg5. These studies supported the unique specificity of BRD9876 for phosphorylated, microtubule-bound Eg5.

BRD9876 Exhibits Improved Selectivity over Hematopoietic Progenitors

Having uncovered a distinct mode of Eg5 inhibition by BRD9876, we investigated whether BRD9876 has unique MM versus hematopoietic selectivity. Indeed, BRD9876 exhibited approximately 3-fold selectivity for MM1S myeloma cells (IC_{50} $3.1 \pm 0.7 \mu\text{M}$) over CD34+ derived hematopoietic cells ($9.1 \pm 2 \mu\text{M}$), whereas the $\alpha 4/\alpha 6$ -binding BI8 exhibited greater inhibition of CD34 cells ($24.7 \pm 1 \mu\text{M}$) than MM1S cells ($57.6 \pm 11.2 \mu\text{M}$; Figure 6A). The loop-L5-binding inhibitors likewise inhibited CD34 growth more than MM1S cells including the low-potency monastrol (CD34: $28.9 \pm 5.0 \mu\text{M}$; MM1S: $143.6 \pm 101 \mu\text{M}$) and the high-potency ispinesib (CD34: $4.5 \pm 1.0 \text{ nM}$; MM1S: $12.6 \pm 2.1 \text{ nM}$). ARRY-520, which is currently in clinical trials for treating MM, binds the loop L5 region (Woessner et al., 2009), and like ispinesib and monastrol, ARRY-520 inhibited CD34 growth more potently (IC_{50} $1.3 \pm 0.4 \text{ nM}$) than MM1S cells ($4.9 \pm 0.2 \text{ nM}$), consistent with the severe hematological toxicity observed in MM patients treated with ARRY-520 (Shah et al., 2011). On the other hand, the ATP-competitive Eg5 inhibitor, GSK1, preferentially inhibits the microtubule-bound form of Eg5 (Luo et al., 2007) like BRD9876 and displayed similar potencies of growth inhibition for both CD34 and MM1S cells. Greater selectivity for MM1S cells was likely not observed because these cells contain >10 -fold greater ATP levels than CD34 cells, measured by the Cell Titer Glo assay.

We verified these selectivity patterns of BRD9876 and ispinesib on a panel of MM and lymphoma cell lines compared with CD34 cells (Figure 6B). Whereas the majority of tested cancer cell lines were less sensitive than CD34 cells to ispinesib's cytotoxicity, all cell lines had greater sensitivity to BRD9876 than CD34 cells. Other MM cell lines AMO-1 and KMS11 also exhibited G2/M arrest with BRD9876 treatment, confirming the same mechanism of action against these cell lines (Figure S7A). Altogether, ATP non-competitive inhibition of microtubule-

bound Eg5 by BRD9876 exclusively allowed selective inhibition of myeloma over CD34 cells.

We determined whether BRD9876's selectivity was due to different growth rates of cancer cell lines and hematopoietic cells. CD34+ cells were co-cultured with OP9 stromal cells that are known to markedly increase growth rates of these cells (Feugier et al., 2005). After 9 days, OP9-co-cultured hematopoietic cells were >10 -fold greater than cells grown alone in cytokine-supplemented media (Figure S7B). However, this increase in growth rate was not accompanied by an increase in sensitivity to 3 days of BRD9876 exposure (Figure S7C). We next determined whether subpopulations of hematopoietic cells had differential sensitivity to BRD9876 using immuno-phenotyping. After 3 days of exposure to BRD9876, there was a slight enrichment of CD34+ cells (16%–22.5%) and a slight decrease in cells weakly expressing myeloid markers (from 26.4% to 14.6%) but no change in cells expressing erythroid markers or cells strongly expressing myeloid markers (Figure S7D). Few cells ($<5\%$) expressed megakaryocytic markers (CD41) or lymphoid markers (CD3 and CD19) and were not analyzed.

In these experiments, hematopoietic progenitors were grown in serum-free liquid culture media for ease of handling, comparability to MM cell line growth-inhibition assays, and amenability to high-throughput testing. "Gold standard" assays to measure hematopoietic toxicity are colony-forming assays in semi-solid media that are predictive of drug doses causing myelosuppression in vivo (Parchment et al., 1998). Doses that cause dose-limiting neutropenia in vivo are correlated to IC_{90} concentrations in granulocyte-macrophage colony-forming unit (CFU-GM) assays in vitro (Pessina et al., 2003). We tested BRD9876 and ispinesib on colony formation of CD34+ progenitors grown in cytokine-supplemented methylcellulose media (Figure 7A), and dose-response relationships were found to be comparable to CD34 cells grown in liquid culture (Figure 6A). Whereas BRD9876 began suppressing erythroid colonies (BFU-E) at $10 \mu\text{M}$, suppression of myeloid (CFU-GM) colonies was only noted at $20 \mu\text{M}$. These data suggest that concentrations of BRD9876 that suppress MM cell line growth (2 – $10 \mu\text{M}$) are unlikely to cause significant myeloid toxicity (neutropenia) in vivo.

Finally, we determined whether phospho-Eg5 levels, which are associated with BRD9876 activity, are different between MM and hematopoietic cells. Indeed, cultured MM1S myeloma cells had \sim 3-fold higher levels of phospho-Eg5 than cultured CD34 cells (Figures 7B and 7C). Similar differences were found between other cultured MM cell lines and CD34 cells (Figure S7E). To exclude the possibility that these differences arose because of the different culture conditions of the two cell types, we tested uncultured CD138+ primary MM cells or CD34+ hematopoietic progenitors isolated from human bone marrow aspirates. Even larger differences (\sim 10-fold) in phospho-Eg5 levels were found between these uncultured MM and hematopoietic cells (Figures 7B and 7C). We tested a larger panel of different

presence of varying concentrations of BRD9876 (top) or ispinesib (bottom), and ATP consumption by Eg5 was quantified. Data are avg \pm SEM of 6 (three experiments).

(E) Y104C mutation is sufficient to confer resistance to BRD9876. SW48 cells were transduced with pLX-TRC312 lentiviruses containing C-terminal GFP-tagged Eg5 open reading frame with the WT sequence (black), Y014C mutation (red), or D130V mutation (blue) and then exposed to BRD9876 (top) or ispinesib (bottom) for 3 days. Cells expressing GFP-tagged Eg5 were quantified by MetaXpress. Data are avg \pm SEM of 4 (two experiments).

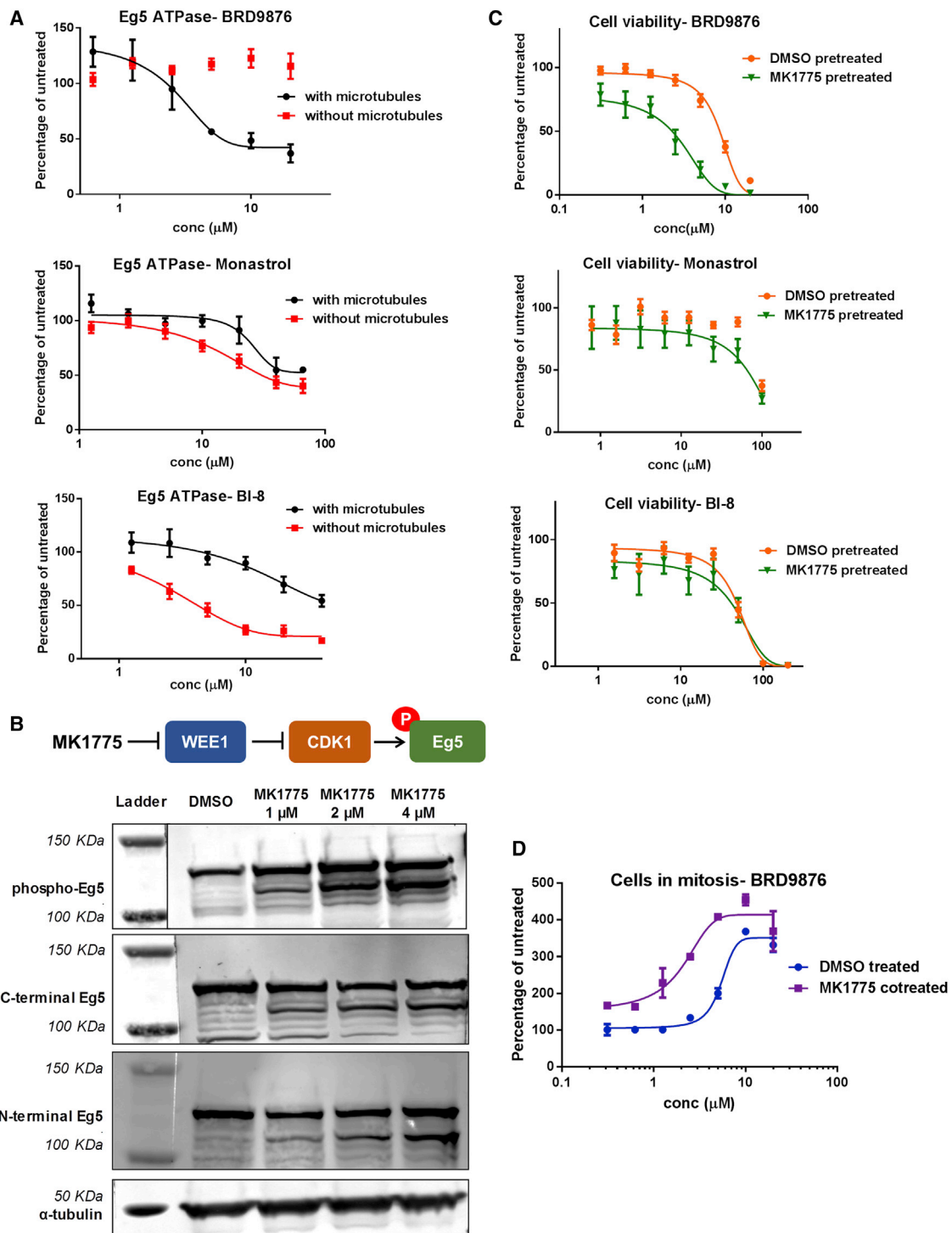


Figure 5. BRD9876 Inhibits Only Microtubule-Bound Eg5

(A) BRD9876 is only active against microtubule-bound Eg5. ATPase activity of Eg5 motor domain was measured in the presence (black) or absence (red) of microtubules with BRD9876 (top), monastrol (middle), or BI-8 (bottom). Data are avg \pm SEM (n = 4).

(B) Eg5 phosphorylation can be increased by using a WEE1 inhibitor. Top: schematic showing how MK1775's inhibition of WEE1 releases inhibition of CDK1, thus increasing Eg5 phosphorylation. Bottom: MM1S cell lysates treated with DMSO or increasing doses of MK1775 for 24 hr were resolved on a 3%–8% tris-acetate gel and immunoblotted with antibodies recognizing Thr927 phosphorylated Eg5 (top), Eg5 C-terminal (middle), Eg5 N-terminal (bottom), or α -tubulin (far bottom). Images were acquired with the LI-COR Odyssey CLX system. A faster migrating band, visible with all three antibodies, intensifies with increasing MK1775 doses and likely represents phospho-Eg5.

(legend continued on next page)

patient-derived CD138+ primary MM cells compared with CD34+ hematopoietic progenitors from different healthy donors (Figure 7D). In all comparisons, the phospho-Eg5 band was consistently higher in freshly isolated MM cells than hematopoietic progenitors, indicating that elevated phospho-Eg5 occurs *in vivo* in MM cells and is conserved across different MM cell types and altogether suggesting that the mode of Eg5 inhibition by BRD9876 may have a significant therapeutic index *in vivo*.

DISCUSSION

In this study, we used the clinically desirable phenotypes of overcoming stromal resistance in multiple myeloma and sparing hematopoietic progenitors and identified a distinct mechanism of Eg5 inhibition. A phenotypic approach identified the first Eg5 inhibitor monastrol and revealed its target Eg5 as a viable therapeutic target (Mayer et al., 1999). This led to the development of a number of Eg5 inhibitors, and one such inhibitor ARRY-520 is now in phase III trials against MM (Owens, 2013). ARRY-520 leads to durable responses in MM patients (Shah et al., 2011), suggesting that this class of inhibitors can overcome stromal resistance. This is likely because very little signal transduction occurs during mitosis from the cell surface to the nucleus (as evidenced by the sparse transcriptional changes induced by BRD9876 in Figure S4A), therefore making it difficult for cancer cells arrested in mitosis to turn on survival pathways using external stromal signals. Existing Eg5 inhibitors are clinically limited by severe (grade 3 or 4) neutropenia (Burriss et al., 2011; Shah et al., 2011), and it was not known until this report whether this toxicity could be mitigated. Using the phenotype of sparing hematopoietic cells, we uncovered a unique mode of Eg5 inhibition through the binding of BRD9876 to a distinct allosteric site on phosphorylated, microtubule-bound form of Eg5. Human hematopoietic cells are relatively spared in this approach, likely because they contain less phosphorylated (microtubule-bound) Eg5. Conversely, greater proportions of unphosphorylated (non-microtubule-bound) Eg5 in hematopoietic cells may increase their susceptibility to current inhibitors such as monastrol, ispinesib, and ARRY-520 (Figure 6A), which preferentially inhibit the free form of Eg5 (Lad et al., 2008; Luo et al., 2004). Hence, inhibition of the same target can have different selectivity outcomes depending on the mode of inhibition.

There are three features unique to BRD9876's inhibition of Eg5 activity: (1) interaction with the tyrosine 104 residue that is part of the α 4- α 6 allosteric binding pocket; (2) microtubule-dependent inhibition; and (3) ATP non-competitive inhibition. Benzimidazole-8 binds the α 4- α 6 pocket (Ulaganathan et al., 2013) but preferentially inhibits the free form of Eg5 (Figure 5A) and displays greater toxicity toward hematopoietic cells (Figure 6A). ATP-competitive inhibitors of Eg5 like GSK1 (Luo et al., 2007) that bind the α 4- α 6 pocket are specific for microtubule-bound protein but do not inhibit MM1S cells more potently than CD34 cells (Figure 6A), likely because MM cells contain higher levels

of ATP. We are unaware of any inhibitor of Eg5 with the unique properties of BRD9876 thus far (although a wide variety of Eg5 inhibitors have been developed by pharmaceutical companies; El-Nassan, 2013). BRD9876 is a tool compound and is not likely to be a drug candidate, given its simple structure and lack of medicinal chemistry opportunities for optimization (Figure S3). It is important to recognize that a number of additional steps (medicinal chemistry to optimize physicochemical properties, pharmacokinetic analyses, *in vivo* efficacy testing, comprehensive toxicity profiling, etc.) are required before a compound with BRD9876's mechanism of action can be a therapeutic candidate. But just as the tool compound monastrol led to the development of optimized loop-L5-binding drug candidates like ispinesib and ARRY-520, our findings indicate that a new generation of Eg5 drug candidates with BRD9876-like mechanism of action should be developed and prioritized for clinical testing based on their potential for lower hematological toxicity.

We noted that hematological toxicities were not reported in murine xenograft studies describing the use of Eg5 inhibitors like ispinesib and ARRY-520 (Purcell et al., 2010; Woessner et al., 2009), even though the dose-limiting toxicity for these and other Eg5 inhibitors is severe (grade 4) neutropenia in human studies (Burriss et al., 2011; Shah et al., 2011). This is likely because murine hematopoietic cells are generally more resistant than human hematopoietic cells to commonly used anti-cancer drugs (that cause neutropenia in humans) with distinct mechanisms such as irinotecan (Erickson-Miller et al., 1997), paclitaxel (Kurtzberg et al., 2009), and fludarabine (Bagley et al., 2009). We therefore deprioritized testing BRD9876 in murine models because it would be difficult to demonstrate the advantage of BRD9876 in sparing hematopoietic progenitors in murine models. Instead, we demonstrated that, unlike other Eg5 inhibitors, efficacious doses of BRD9876 spare human hematopoietic progenitors in the CFU-GM assay (Figure 7A), which is more predictive of human hematological toxicity (Parchment et al., 1998; Pessina et al., 2003). Altogether, Eg5 inhibitors with BRD9876-like mechanisms of action may display a greater therapeutic index (difference between efficacious and toxic doses) than existing Eg5 inhibitors in human studies, but not in preclinical xenograft models.

The advantage of improving the therapeutic index of Eg5 inhibitors can be inferred from promising clinical trial results of ARRY-520 in MM. Because neutropenia was the dose-limiting toxicity early in phase I testing, patients were treated with granulocyte colony-stimulating factor (G-CSF) support that boosts neutrophil counts (Shah et al., 2011). This allowed a higher maximal tolerated dose to be administered to patients and longer durations of treatment. Clinical investigators reported that the median time to response with ARRY-520 was noticeably prolonged (3.7 months; Shah et al., 2011), consistent with the primarily cytostatic effects of Eg5 inhibition. In most clinical trials with Eg5 inhibitors in which G-CSF support was not used, treatment durations were short, which may have precluded

(C) Increasing Eg5 phosphorylation by MK1775 pretreatment only enhances BRD9876's cytotoxic activity. MM1S cells were pretreated with 0.5 μ M MK-1775 for 24 hr and then treated with BRD9876 (top), monastrol (middle), or BI-8 (bottom) for 3 days. Data are avg \pm SEM ($n \geq 4$; greater than or equal to two experiments). (D) Increasing Eg5 phosphorylation enhances mitotic arrest by BRD9876. MM1S cells co-treated with 0.5 μ M MK1775 and varying concentrations of BRD9876 for 24 hr were stained for the mitotic marker phospho-histone H3 (S10). Data are avg \pm SEM ($n = 4$).

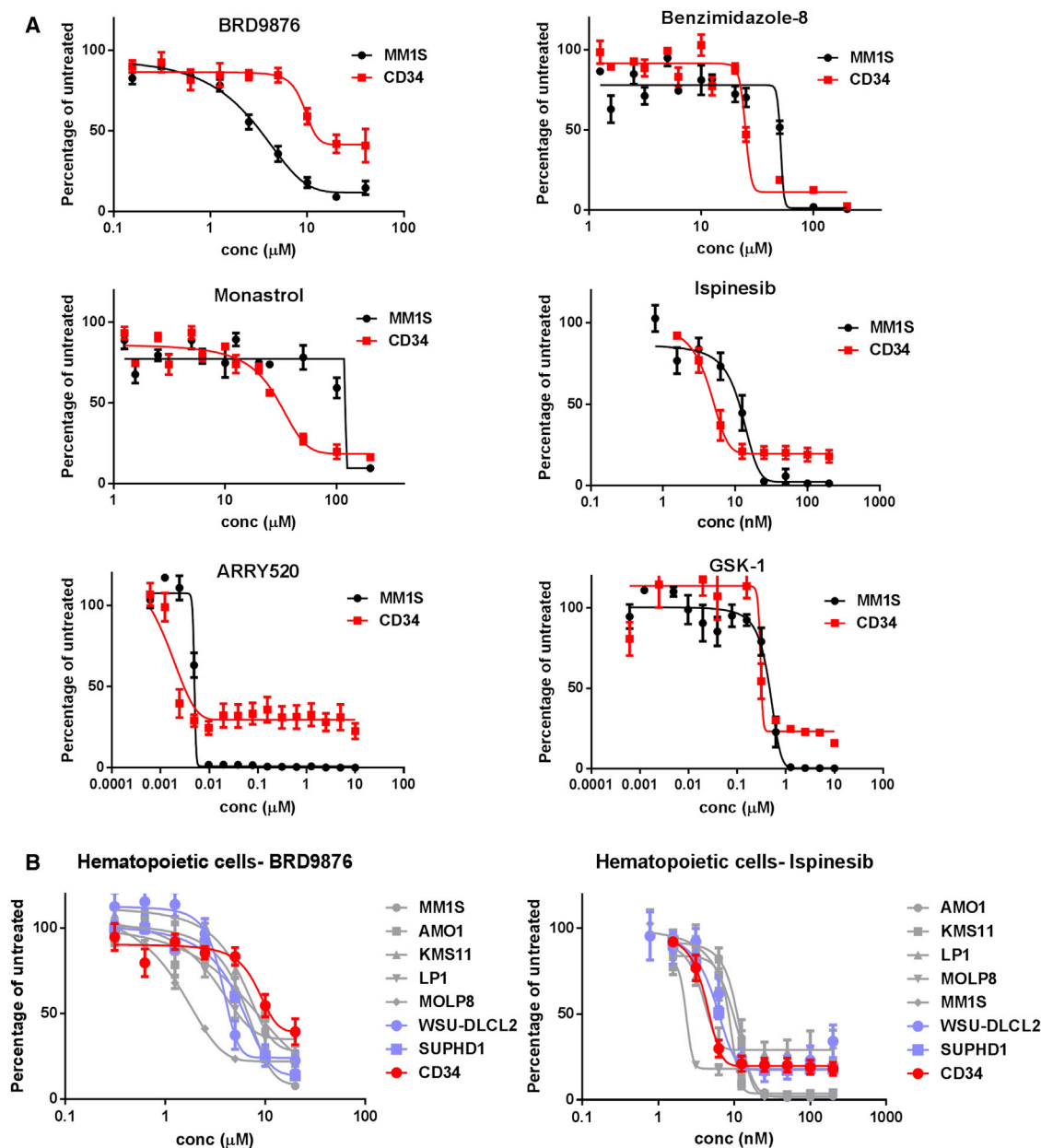


Figure 6. BRD9876 Exhibits Improved Selectivity between Myeloma Cells and Hematopoietic Progenitors

(A) BRD9876 has unique selectivity for MM over hematopoietic cells. MM1S cells (black) and CD34⁺-derived hematopoietic cells (red) were exposed to various concentrations of BRD9876 (top left), BI-8 (top right), monastrol (middle left), ispinesib (middle right), ARRY-520 (bottom left), or GSK-1 (bottom right) for 3 days and then viability measured with Cell Titer Glo. Data are avg \pm SEM ($n \geq 4$; greater than or equal to two experiments).

(B) Improved cancer/normal selectivity with BRD9876. The indicated MM cell lines (gray), lymphoma cell lines (blue), or normal hematopoietic cells (red) were exposed to BRD9876 (left) or ispinesib (right) for 3 days and then viability was measured with Cell Titer Glo. Data are avg \pm SEM ($n \geq 6$; greater than or equal to three experiments).

demonstration of responses resulting from Eg5 inhibition. For example, in a recent phase II trial of the Eg5 inhibitor AZD4877 in urothelial cancers (Jones et al., 2013), the median treatment duration was only 43 days (~ 1.5 months) and no responses were noted. Because lowering neutropenia allowed higher doses, greater treatment duration, and the demonstration of efficacy with ARRY-520, further lowering of neutropenia with the

specific mode of Eg5 inhibition we identified (combined with G-CSF support) has the potential to improve further outcomes of patients treated with this approach.

An additional discovery resulting from our study is the consistently higher proportion of phospho-Eg5 in MM cells, particularly in various types of patient-derived CD138⁺ cells, compared to non-malignant hematopoietic progenitors. Whereas the simplest

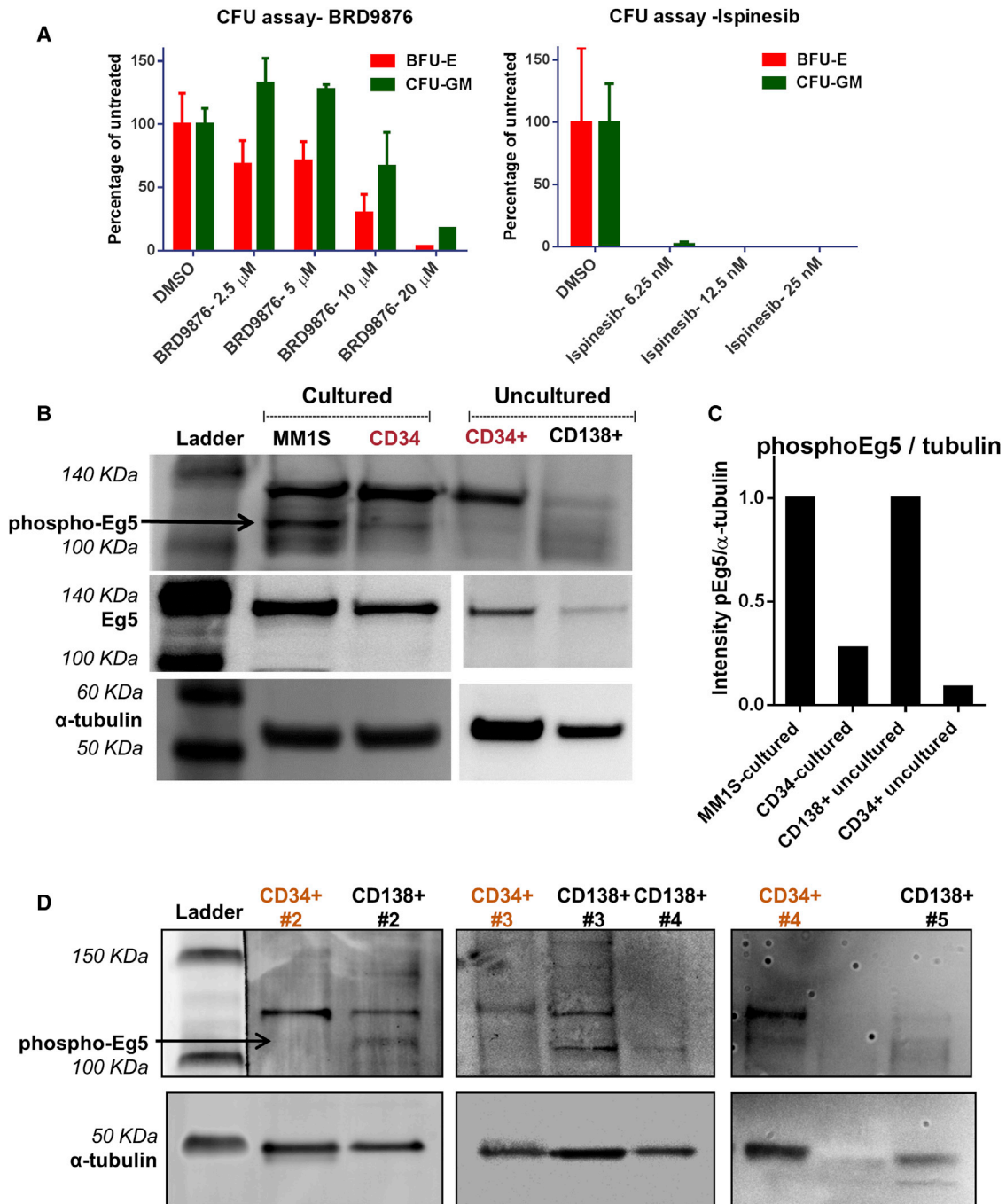


Figure 7. BRD9876 Spares Colony Formation of Hematopoietic Progenitors, which Contain Lower Phosphorylated Eg5 Than Myeloma Cells

(A) CD34⁺ hematopoietic progenitors were cultured for 14 days in serum-free semi-solid methylcellulose media supplemented with erythroid and myeloid growth factors (Methocult H4436) in the presence of BRD9876 (left) or ispinesib (right). Erythroid (CFU-E) and myeloid (CFU-GM) colonies were then quantified by manual counting. Data are avg \pm SEM (n = 4; two experiments).

(B) MM cells have higher phosphorylated Eg5 than hematopoietic cells. Lysates of equal numbers of cultured MM1S cells, CD34⁺ hematopoietic cells cultured for 7 days, uncultured CD34⁺ cells, or uncultured CD138⁺ MM cells from a patient were subjected to immunoblotting for Thr927-phosphorylated Eg5, total Eg5, or α -tubulin using chemiluminescence detection. Arrow indicates the faster migrating phospho-Eg5 band.

(C) Quantification of intensities of the faster migrating phospho-Eg5 band and its physiological substrate α -tubulin from (B) was done using Kodak Carestream software and expressed as ratios of phospho-Eg5/ α -tubulin. Data were normalized to MM ratios for each condition (cultured MM1S or uncultured CD138⁺ MM cells).

(D) Differences in phosphorylated Eg5 between primary MM and hematopoietic cells are generalizable. Equal numbers of primary CD138⁺ cells from MM patients or CD34⁺ cells from healthy donors (Lonza) were compared in immunoblots for phospho-Eg5 (top) or α -tubulin (bottom) using either LI-COR fluorescence detection (left and middle panels) or chemiluminescence (right panel). Arrow indicates the phospho-Eg5 band.

explanation is a higher growth fraction of MM cells, increasing the growth rate of hematopoietic cells did not affect sensitivity to BRD9876 (Figure S7C). Furthermore, the mitotic rate of MM cells in patients is not high, as evidenced by the limited efficacy of microtubule-targeting anti-mitotic drugs like paclitaxel in MM (Dimopoulos et al., 1994). It is possible that MM cells have greatly activated CDK1 (CDC2), which phosphorylates Eg5, beyond physiological levels of mitotic activation. Chromosomal abnormalities are universal in MM (Zandecki et al., 1996), and chromosomal instability can cause excessive activation of the spindle assembly checkpoint, which is known to occur in MM (Decaux et al., 2008). Sustained spindle assembly checkpoint causes prolonged stabilization of cyclin B, the activating partner of CDK1 (Musacchio and Salmon, 2007). Thus, excessive CDK1 activation could occur commonly in MM, leading to high phospho-Eg5, which can be selectively exploited by BRD9876.

In summary, our study has identified small molecules that overcome the stromal resistance phenotype in MM. These small molecules will be critical to uncover additional “druggable” vulnerabilities within MM. This phenotypic chemical-biology approach complements current genetic approaches of discovering new therapeutic strategies against multiple myeloma, hopefully leading us closer to the eradication of this disease.

EXPERIMENTAL PROCEDURES

All experimental procedures are described in detail in [Supplemental Information](#).

Cell Culture and Screening

MM cell lines MM.1S, INA6, and MOLP5 were grown in RPMI media supplemented with 10% fetal bovine serum and grown alone (MM.1S) with 2 ng/ml IL6 (INA6) or in co-culture with primary human BMSCs (MOLP5). For identification in co-cultures, these MM cell lines were stably transduced with a GFP-expressing lentivirus. Frozen CD34+ human bone marrow hematopoietic progenitors (Lonza) were cultured in serum-free HPGM medium (Lonza) supplemented with 50 ng/ml thrombopoietin, 50 ng/ml FLT3 ligand, and 25 ng/ml Stem Cell Factor. Cells derived from CD34+ cells were used for experiments 1 week after thawing.

For primary screening, GFP-labeled MOLP5 cells were co-cultured with unlabeled BMSCs in 384-well plates for 2 days and then exposed to compounds at a single concentration (10 μ M) in duplicate or DMSO controls for 3 days. Remaining GFP(+) MOLP5 cells were quantified by high-throughput microscopy (IXMicro; Molecular Devices), counting GFP(+) cells with the MetaXpress software (Molecular Devices). For counter-screening, BMSCs alone were exposed to hit compounds at 10 μ M for 3 days and viability measured using Cell Titer Glo reagent (Promega). In secondary assays, GFP(+) MM1S or INA6 cells were grown alone or co-cultured with BMSCs in 384-well plates and exposed to eight doses of compounds for 3 days followed by image-based quantification. For validation, compounds were ordered in dry powder form from commercial vendors, re-dissolved in DMSO, and re-tested on growth inhibition assays. For tertiary screening, compounds at eight doses were tested on CD34 hematopoietic cells for 3 days and viability measured using Cell Titer Glo. For final validation, primary MM cells were isolated from bone marrow aspirates using CD138 immunomagnetic selection, co-cultured with primary BMSCs, and exposed to eight doses of compounds for 3 days. Viable cells were quantified using 2 μ M Calcein AM staining and imaging.

Gene Expression Analysis

MM1S cells were exposed to either 10 μ M BRD9876 or DMSO for 6 hr, following which RNA was extracted using the TRIzol reagent (Invitrogen). Hybridization on Affymetrix human U133 2.0 plus microarrays chips was performed and results were analyzed with the Comparative Marker Selection

algorithm of GenePattern (<http://www.broadinstitute.org/cancer/software/genepattern>).

Cell Cycle Analysis

MM1S or CD34 cells were exposed to 10 μ M BRD9876 or DMSO, fixed with 70% ethanol, stained with propidium iodide, and analyzed with the FACSCalibur (BD Biosciences) instrument. Cell cycle analysis was performed with the Watson modeling within Flowjo v7 software (Tree Star).

Eg5 Biochemical Assays

Microtubule gliding assays of full-length Eg5 were performed as previously described (Mayer et al., 1999). To measure ATPase activity, recombinant GST-tagged Eg5 motor domain (amino acid 1–368) proteins with the wild-type sequence or Y104C or D130V mutations were generated. Microtubule-stimulated ATPase activity was initially measured using the ELIPA kit (Cytoskeleton) in 96-well plates. In later experiments, the Eg5 ATPase assay was performed in 384-well plates in PEM25 buffer (Luo et al., 2004) using the ADP-Glo reagent (Promega) to detect ATP hydrolysis. ATP competition was measured by varying concentrations of ATP (12.5–800 μ M) and BRD9876 (0, 1.25, 5, and 20 μ M) in Eg5 ATPase assays. Data were analyzed by double-reciprocal Lineweaver-Burk plots, Michaelis-Menten plots, or mixed-model inhibition analyses all using GraphPad Prism 6.

Human Hematopoietic Progenitor Colony-Forming Cell Assays

Colony-forming assays for human bone marrow CD34+ hematopoietic progenitors (Lonza) were performed using the Methocult H4436 Enriched kit (Stem Cell Technologies) with varying concentrations of Eg5 inhibitors or DMSO. Erythroid or granulocyte colonies formed after 14 days were manually counted with a 4 \times objective and 60-mm gridded scoring dish.

ACCESSION NUMBERS

The GEO accession number for the gene expression analysis data presented in this paper is GSE64178.

SUPPLEMENTAL INFORMATION

Supplemental Information includes Supplemental Experimental Procedures, seven figures, and one table and can be found with this article online at <http://dx.doi.org/10.1016/j.celrep.2015.01.017>.

AUTHOR CONTRIBUTIONS

Project strategy was provided by S.C., A.L.S., S.M., K.A.H., P.G.M., A.M.S., A.F.S., T.H., B.L.E., M.A.S.M., T.R.G., N.S.R., D.T.S., and S.L.S. Assay development was provided by S.C., A.L.S., S.M., L.C.C., N.J.T., S.V., and A.M.S. Screening was provided by S.C., A.L.S., L.C.C., and N.J.T. Follow-up studies were provided by S.C., C.H., R.S., R.Z.Y., D.B.S., J.P., A.V., L.S., D.D.C., J.I., and R.K. Chemistry was provided by M.M.M., M.M.H., S.S., and R.Q. Informatics were provided by V.D. and P.A.C. Manuscript drafting was provided by S.C. and S.L.S.

ACKNOWLEDGMENTS

We wish to thank T. Hasaka, J. Bradner, T. Kapoor, L. VerPlank, M. Bliss-Moreau, V. Raksakulthai, J. Negri, M. Palmer, J. Burbank, P. Aspesi, Jr., D. Barker, K. Emmith, J. Bittker, B. Wagner, J. Perez, J. Cheah, E. Price, S. Johnston, G. Walzer, Z. Boskovic, D. Walpita, A. Bracha, C. Hon, J. McGrath, C. Hartland, J. Kotz, R. Bejar, I. Pomerantseva, J. Vacanti, S. Pozzi, N. Vaghela, K. Patel, J. Schoonmaker, K. Maxcy, Broad Compound Management, and the S.L.S., D.T.S., and N.S.R. laboratories for scientific discussions, technical expertise, and/or reagents. This work was funded by grants from the Starr Cancer Consortium, the NIH awards R01GM038627 (to S.L.S.), RL1HG004671 (to S.L.S.), R01DK050234 (to D.T.S.), U54CA163191 (to D.T.S.), K08CA158149 (to S.C.), P50CA100707 Dana-Farber/ Harvard Cancer Center Multiple Myeloma S.P.O.R.E. career development sub-award (to S.C.), and the Multiple Myeloma

Research Foundation Research Fellow Award (to S.C.). The content of this publication is solely the responsibility of the authors and does not necessarily reflect the views or policies of the Department of Health and Human Services, nor does mention of trade names, commercial products, or organizations imply endorsement by the US government. T.R.G. and S.L.S. are Investigators at the Howard Hughes Medical Institute.

Received: November 19, 2014

Revised: December 17, 2014

Accepted: January 6, 2015

Published: February 5, 2015

REFERENCES

- Adams, J., Behnke, M., Chen, S., Cruickshank, A.A., Dick, L.R., Grenier, L., Klunder, J.M., Ma, Y.T., Plamondon, L., and Stein, R.L. (1998). Potent and selective inhibitors of the proteasome: dipeptidyl boronic acids. *Bioorg. Med. Chem. Lett.* **8**, 333–338.
- Alberts, D.S., and Salmon, S.E. (1975). Adriamycin (NSC-123127) in the treatment of alkylator-resistant multiple myeloma: a pilot study. *Cancer Chemother. Rep.* **59**, 345–350.
- Bagley, R.G., Roth, S., Kurtzberg, L.S., Rouleau, C., Yao, M., Crawford, J., Krumbholz, R., Lovett, D., Schmid, S., and Teicher, B.A. (2009). Bone marrow CFU-GM and human tumor xenograft efficacy of three antitumor nucleoside analogs. *Int. J. Oncol.* **34**, 1329–1340.
- Bartlett, J.B., Dredge, K., and Dalgleish, A.G. (2004). The evolution of thalidomide and its IMiD derivatives as anticancer agents. *Nat. Rev. Cancer* **4**, 314–322.
- Blangy, A., Lane, H.A., d'Hérin, P., Harper, M., Kress, M., and Nigg, E.A. (1995). Phosphorylation by p34cdc2 regulates spindle association of human Eg5, a kinesin-related motor essential for bipolar spindle formation in vivo. *Cell* **83**, 1159–1169.
- Burris, H.A., 3rd, Jones, S.F., Williams, D.D., Kathman, S.J., Hodge, J.P., Pandite, L., Ho, P.T., Boerner, S.A., and Lorusso, P. (2011). A phase I study of ispinesib, a kinesin spindle protein inhibitor, administered weekly for three consecutive weeks of a 28-day cycle in patients with solid tumors. *Invest. New Drugs* **29**, 467–472.
- Chatterjee, M., Hönemann, D., Lentzsch, S., Bommert, K., Sers, C., Herrmann, P., Mathas, S., Dörken, B., and Bargou, R.C. (2002). In the presence of bone marrow stromal cells human multiple myeloma cells become independent of the IL-6/gp130/STAT3 pathway. *Blood* **100**, 3311–3318.
- Dalton, W., and Anderson, K.C. (2006). Synopsis of a roundtable on validating novel therapeutics for multiple myeloma. *Clin. Cancer Res.* **12**, 6603–6610.
- Decaux, O., Lodé, L., Magrangeas, F., Charbonnel, C., Gouraud, W., Jézéquel, P., Attal, M., Harousseau, J.L., Moreau, P., Bataille, R., et al.; Intergroupe Francophone du Myélome (2008). Prediction of survival in multiple myeloma based on gene expression profiles reveals cell cycle and chromosomal instability signatures in high-risk patients and hyperdiploid signatures in low-risk patients: a study of the Intergroupe Francophone du Myélome. *J. Clin. Oncol.* **26**, 4798–4805.
- Dimopoulos, M.A., Arbutck, S., Huber, M., Weber, D., Lockett, R., Delasalle, K., and Alexanian, R. (1994). Primary therapy of multiple myeloma with paclitaxel (taxol). *Ann. Oncol.* **5**, 757–759.
- El-Nassan, H.B. (2013). Advances in the discovery of kinesin spindle protein (Eg5) inhibitors as antitumor agents. *Eur. J. Med. Chem.* **62**, 614–631.
- Erickson-Miller, C.L., May, R.D., Tomaszewski, J., Osborn, B., Murphy, M.J., Page, J.G., and Parchment, R.E. (1997). Differential toxicity of camptothecin, topotecan and 9-aminocamptothecin to human, canine, and murine myeloid progenitors (CFU-GM) in vitro. *Cancer Chemother. Pharmacol.* **39**, 467–472.
- Fenteany, G., Standaert, R.F., Lane, W.S., Choi, S., Corey, E.J., and Schreiber, S.L. (1995). Inhibition of proteasome activities and subunit-specific amino-terminal threonine modification by lactacystin. *Science* **268**, 726–731.
- Ferlay, J., Soerjomataram, I., Ervik, M., Dikshit, R., Eser, S., Mathers, C., Rebelo, M., Parkin, D.M., Forman, D., and Bray, F. (2013). GLOBOCAN 2012: estimated cancer incidence, mortality and prevalence worldwide in 2012. <http://globocan.iarc.fr>.
- Feugier, P., Li, N., Jo, D.Y., Shieh, J.H., MacKenzie, K.L., Lesesve, J.F., Latger-Cannard, V., Bensoussan, D., Crystal, R.G., Rafii, S., et al. (2005). Osteopetrotic mouse stroma with thrombopoietin, c-kit ligand, and flk-2 ligand supports long-term mobilized CD34+ hematopoiesis in vitro. *Stem Cells Dev.* **14**, 505–516.
- Hideshima, T., Chauhan, D., Shima, Y., Raje, N., Davies, F.E., Tai, Y.T., Treon, S.P., Lin, B., Schlossman, R.L., Richardson, P., et al. (2000). Thalidomide and its analogs overcome drug resistance of human multiple myeloma cells to conventional therapy. *Blood* **96**, 2943–2950.
- Hideshima, T., Richardson, P., Chauhan, D., Palombella, V.J., Elliott, P.J., Adams, J., and Anderson, K.C. (2001). The proteasome inhibitor PS-341 inhibits growth, induces apoptosis, and overcomes drug resistance in human multiple myeloma cells. *Cancer Res.* **61**, 3071–3076.
- Hideshima, T., Mitsiades, C., Tonon, G., Richardson, P.G., and Anderson, K.C. (2007). Understanding multiple myeloma pathogenesis in the bone marrow to identify new therapeutic targets. *Nat. Rev. Cancer* **7**, 585–598.
- Jones, R., Vuky, J., Elliott, T., Mead, G., Arranz, J.A., Chester, J., Chowdhury, S., Dudek, A.Z., Müller-Mattheis, V., Grimm, M.O., et al. (2013). Phase II study to assess the efficacy, safety and tolerability of the mitotic spindle kinesin inhibitor AZD4877 in patients with recurrent advanced urothelial cancer. *Invest. New Drugs* **31**, 1001–1007.
- Kim, E.D., Buckley, R., Learman, S., Richard, J., Parke, C., Worthylake, D.K., Wojcik, E.J., Walker, R.A., and Kim, S. (2010). Allosteric drug discrimination is coupled to mechanochemical changes in the kinesin-5 motor core. *J. Biol. Chem.* **285**, 18650–18661.
- Krajewska, M., Heijink, A.M., Bisselink, Y.J., Seinstra, R.I., Silljé, H.H., de Vries, E.G., and van Vugt, M.A. (2013). Forced activation of Cdk1 via wee1 inhibition impairs homologous recombination. *Oncogene* **32**, 3001–3008.
- Kurtzberg, L.S., Roth, S.D., Bagley, R.G., Rouleau, C., Yao, M., Crawford, J.L., Krumbholz, R.D., Schmid, S.M., and Teicher, B.A. (2009). Bone marrow CFU-GM and human tumor xenograft efficacy of three tubulin binding agents. *Cancer Chemother. Pharmacol.* **64**, 1029–1038.
- Lad, L., Luo, L., Carson, J.D., Wood, K.W., Hartman, J.J., Copeland, R.A., and Sakowicz, R. (2008). Mechanism of inhibition of human KSP by ispinesib. *Biochemistry* **47**, 3576–3585.
- Lamb, J., Crawford, E.D., Peck, D., Modell, J.W., Blat, I.C., Wrobel, M.J., Lerner, J., Brunet, J.P., Subramanian, A., Ross, K.N., et al. (2006). The Connectivity Map: using gene-expression signatures to connect small molecules, genes, and disease. *Science* **313**, 1929–1935.
- Lohr, J.G., Stojanov, P., Carter, S.L., Cruz-Gordillo, P., Lawrence, M.S., Auclair, D., Sounguez, C., Knoechel, B., Gould, J., Saksena, G., et al.; Multiple Myeloma Research Consortium (2014). Widespread genetic heterogeneity in multiple myeloma: implications for targeted therapy. *Cancer Cell* **25**, 91–101.
- Luo, L., Carson, J.D., Dhanak, D., Jackson, J.R., Huang, P.S., Lee, Y., Sakowicz, R., and Copeland, R.A. (2004). Mechanism of inhibition of human KSP by monastrol: insights from kinetic analysis and the effect of ionic strength on KSP inhibition. *Biochemistry* **43**, 15258–15266.
- Luo, L., Parrish, C.A., Nevins, N., McNulty, D.E., Chaudhari, A.M., Carson, J.D., Sudakin, V., Shaw, A.N., Lehr, R., Zhao, H., et al. (2007). ATP-competitive inhibitors of the mitotic kinesin KSP that function via an allosteric mechanism. *Nat. Chem. Biol.* **3**, 722–726.
- Man, C., Rosa, J., Yip, Y.L., Cheung, A.L., Kwong, Y.L., Doxsey, S.J., and Tsao, S.W. (2008). Id1 overexpression induces tetraploidization and multiple abnormal mitotic phenotypes by modulating aurora A. *Mol. Biol. Cell* **19**, 2389–2401.
- Matsuo, Y., Drexler, H.G., Nishizaki, C., Harashima, A., Fukuda, S., Kozuka, T., Sezaki, T., and Orita, K. (2000). Human bone marrow stroma-dependent cell line MOLP-5 derived from a patient in leukaemic phase of multiple myeloma. *Br. J. Haematol.* **109**, 54–63.

- Mayer, T.U., Kapoor, T.M., Haggarty, S.J., King, R.W., Schreiber, S.L., and Mitchison, T.J. (1999). Small molecule inhibitor of mitotic spindle bipolarity identified in a phenotype-based screen. *Science* **286**, 971–974.
- McMillin, D.W., Delmore, J., Weisberg, E., Negri, J.M., Geer, D.C., Klippel, S., Mitsiades, N., Schlossman, R.L., Munshi, N.C., Kung, A.L., et al. (2010). Tumor cell-specific bioluminescence platform to identify stroma-induced changes to anticancer drug activity. *Nat. Med.* **16**, 483–489.
- Meads, M.B., Hazlehurst, L.A., and Dalton, W.S. (2008). The bone marrow microenvironment as a tumor sanctuary and contributor to drug resistance. *Clin. Cancer Res.* **14**, 2519–2526.
- Musacchio, A., and Salmon, E.D. (2007). The spindle-assembly checkpoint in space and time. *Nat. Rev. Mol. Cell Biol.* **8**, 379–393.
- Nielsen, T.E., and Schreiber, S.L. (2008). Towards the optimal screening collection: a synthesis strategy. *Angew. Chem. Int. Ed. Engl.* **47**, 48–56.
- Olaharski, A.J., Uppal, H., Cooper, M., Platz, S., Zabka, T.S., and Kolaja, K.L. (2009). In vitro to in vivo concordance of a high throughput assay of bone marrow toxicity across a diverse set of drug candidates. *Toxicol. Lett.* **188**, 98–103.
- Owens, B. (2013). Kinesin inhibitor marches toward first-in-class pivotal trial. *Nat. Med.* **19**, 1550.
- Parchment, R.E., Gordon, M., Grieshaber, C.K., Sessa, C., Volpe, D., and Ghielmini, M. (1998). Predicting hematological toxicity (myelosuppression) of cytotoxic drug therapy from in vitro tests. *Ann. Oncol.* **9**, 357–364.
- Pessina, A., Albella, B., Bayo, M., Bueren, J., Brantom, P., Casati, S., Croera, C., Gagliardi, G., Foti, P., Parchment, R., et al. (2003). Application of the CFU-GM assay to predict acute drug-induced neutropenia: an international blind trial to validate a prediction model for the maximum tolerated dose (MTD) of myelosuppressive xenobiotics. *Toxicol. Sci.* **75**, 355–367.
- Purcell, J.W., Davis, J., Reddy, M., Martin, S., Samayoa, K., Vo, H., Thomsen, K., Bean, P., Kuo, W.L., Ziyad, S., et al. (2010). Activity of the kinesin spindle protein inhibitor ispinesib (SB-715992) in models of breast cancer. *Clin. Cancer Res.* **16**, 566–576.
- Rath, A., Glibowicka, M., Nadeau, V.G., Chen, G., and Deber, C.M. (2009). Detergent binding explains anomalous SDS-PAGE migration of membrane proteins. *Proc. Natl. Acad. Sci. USA* **106**, 1760–1765.
- Richardson, P.G., Sonneveld, P., Schuster, M.W., Irwin, D., Stadtmauer, E.A., Facon, T., Harousseau, J.L., Ben-Yehuda, D., Lonial, S., Goldschmidt, H., et al.; Assessment of Proteasome Inhibition for Extending Remissions (APEX) Investigators (2005). Bortezomib or high-dose dexamethasone for relapsed multiple myeloma. *N. Engl. J. Med.* **352**, 2487–2498.
- Shah, J.J., Zonder, J., Cohen, A., Orlowski, R.Z., Alexanian, R., Thomas, S.K., Weber, D., Kaufman, J.L., Harvey, R.D., Walker, D., et al. (2011). ARRY-520 shows durable responses in patients with relapsed/refractory multiple myeloma in a phase 1 dose-escalation study. *ASH Annual Meeting Abstracts* **118**, 1860.
- Swinney, D.C., and Anthony, J. (2011). How were new medicines discovered? *Nat. Rev. Drug Discov.* **10**, 507–519.
- Talapatra, S.K., Schüttelkopf, A.W., and Kozielski, F. (2012). The structure of the ternary Eg5-ADP-ispinesib complex. *Acta Crystallogr. D Biol. Crystallogr.* **68**, 1311–1319.
- Tillemont, V., Remy, M.H., Raynaud-Messina, B., Mazzolini, L., Haren, L., and Merdes, A. (2009). Spindle assembly defects leading to the formation of a monopolar mitotic apparatus. *Biol. Cell* **101**, 1–11.
- Ulaganathan, V., Talapatra, S.K., Rath, O., Pannifer, A., Hackney, D.D., and Kozielski, F. (2013). Structural insights into a unique inhibitor binding pocket in kinesin spindle protein. *J. Am. Chem. Soc.* **135**, 2263–2272.
- Vassilev, L.T., Tovar, C., Chen, S., Knezevic, D., Zhao, X., Sun, H., Heimbrook, D.C., and Chen, L. (2006). Selective small-molecule inhibitor reveals critical mitotic functions of human CDK1. *Proc. Natl. Acad. Sci. USA* **103**, 10660–10665.
- Woessner, R., Tunquist, B., Lemieux, C., Chlipala, E., Jackinsky, S., Dewolf, W., Jr., Voegtli, W., Cox, A., Rana, S., Lee, P., and Walker, D. (2009). ARRY-520, a novel KSP inhibitor with potent activity in hematological and taxane-resistant tumor models. *Anticancer Res.* **29**, 4373–4380.
- Zandecki, M., Lai, J.L., and Facon, T. (1996). Multiple myeloma: almost all patients are cytogenetically abnormal. *Br. J. Haematol.* **94**, 217–227.
- Zhang, J.H., Chung, T.D., and Oldenburg, K.R. (1999). A simple statistical parameter for use in evaluation and validation of high throughput screening assays. *J. Biomol. Screen.* **4**, 67–73.
- Zlei, M., Egert, S., Wider, D., Ihorst, G., Wäsch, R., and Engelhardt, M. (2007). Characterization of in vitro growth of multiple myeloma cells. *Exp. Hematol.* **35**, 1550–1561.